Erosion processes in black marl soils at the millimetre scale: preliminary insights from an analogous model

J. Bechet[1], J. Duc[1], M. Jaboyedoff[1], A. Loye[1] and N. Mathys[2]

[1]{University of Lausanne, Risk-group - ISTE - Institute of Earth Sciences, Lausanne, Switzerland}

[2]{ IRSTEA Grenoble, Unité de recherche Erosion Torrentielle, Neige et Avalanches, BP 76, 38402 Saint Martin d'Hères, France }

Correspondence to: M. Jaboyedoff (michel.jaboyedoff@unil.ch)

Abstract

To investigate the millimetre-scale surface processes caused by natural rainfall, an undisturbed sample of badlands soil (1 m long, 0.5 m wide and 0.15 m thick) was carefully extracted. The sample is composed of black marl soil from a badlands area of the Draix Observatory (SE France). After extraction, the undisturbed sample was placed at the same slope angle (45°) as its original orientation and was then monitored for several processes via a terrestrial laser scanner (TLS) with millimetre-scale accuracy and resolution. This experiment identified several surface processes interpreted as micro-landslides, swelling of the black marl material and lateral expansion that closed desiccation cracks. These micro-processes illustrate the complexity of the surface micro-topography changes that control erosion and infiltration rates over time.

1 Introduction

Small black marl watersheds have strong responses to climate forcing (Malet et al., 2007). This study aims to better understand the erosional behaviour and the micro-morphological evolution of these materials caused by micro-scale mass movements in response to precipitation. The goal of this experiment was to extract an undisturbed sample of black marl and expose this material to a natural rainfall event in order to monitor the sample's surface evolution using a 3D laser scanner. This monitoring has permitted us to study the micro-topographic surface deformation and erosion processes that may have an impact on infiltration rates during rainfall events (Mitchell and van Genuchten, 1993; Römkens and

Prasad, 2006). In addition, these surface changes may also play a role in the triggering of landslides (Galeandro et al., 2014). Contrary to the original intention, the duration of the experiment and the rainfall intensity did not permit investigation of splash erosion, which can be important when rainfall is intense (Selby, 1993), because its effect was below the resolution of our acquisition and because the intensity of the rainfall was rather low.

In the past, several studies of artificial rain simulations have been performed at the Draix Observatory (ORE Draix), which is dedicated to the research of mountain hydrology and erosional processes. Previous studies focused on the measurement of sediment transport (Oostwoud Wijdenes and Ergenzinger, 1998) and runoff as a function of precipitation (Mathys et al., 2005). The badlands ground surface evolution has already been monitored during rainfall simulations by using a pin-type micro-relief meter and photography (Torri et al., 1999; Mathys et al., 2005), but these tools were not able to reach the same precision as a laser scanner. Recent studies have shown the potential for observing and characterizing erosional processes at the level of micro-topography using a laser scanner (Schmid et al., 2004; Barneveld et al., 2013).

The soil sample was extracted from the Draix experimental site (ORE Draix, IRSTEA), a badlands area near the city of Digne-les-Bains in the southern French Alps. The experiment was performed in Lausanne (Switzerland), where the precipitation is similar to the Alpine region. For the monitoring of the sample surface, a terrestrial laser scanner (TLS) was used to (1) identify the millimetre-scale processes that control erosion and infiltration by (2) quantifying the swelling of the material in the marls during rainfall events and (3) mapping all possible modifications of the terrain surface.

2 Geological setting

The badlands near the village of Draix are composed of weathered black marls of Middle Jurassic age (Callovo-Oxfordian). The black marl formation is more than 2,000 m thick in certain places (Antoine *et al*., 1995). The study site has no vegetal cover, and the regolith is usually approximately 40 cm to 1 m thick (Maquaire et al., 2002; Antoine et al., 1995). The upper approximately 10 cm of the regolith is loose detrital material composed of local clasts and platelets (Maquaire et al., 2002). This regolith corresponds to a sandy loam when it has been exposed for long enough to be disaggregated by weathering (Antoine et al., 1995). When the upper regolith layer is fresh, it can be considered loamy sand or sand. Below the regolith is a layer of plate-like unstructured rock. Finally, compacted regolith 10 to 20 cm thick lies in contact with the bedrock (Maquaire et al., 2002). The clay size fraction of the black marls located in this region has been found to be 35±5% (Caris et Van Asch, 1991), but the clay mineral content is approximately 10% and is primarily illite with traces of smectite and interstratified clay minerals (Antoine et al., 1995). During rainfall events, water infiltrates the ground, and the material swells because of the behaviour of the fine-grained material and chemical reactions (Antoine et al., 1995). The loose upper-layer detrital material is very sensitive to erosion and is a good candidate for experiments involving surface processes imaging.

3 Methods

3.1 Samples

The sample of soil used for this experiment was extracted from a marl outcrop with a 45° slope. The bedding is nearly normal to the face of the outcrop (Figure 1a). Nevertheless, the loose detrital material at the surface does not display any identifiable bedding structure. The sample is 1 m long, 0.5 m wide and 0.15 m thick. To extract this sample of soil, a metal case was designed to keep the soil structure undisturbed (Figure 1). The extraction was performed by pressing the bottomless box into the ground and inserting the bottom plate via tapping with a hammer to isolate a sample of the upper part of the regolith. This sample was stored in the laboratory in dry conditions, which were similar to natural conditions, for 3 months before the experiment started.

3.2 Experiment design

On 31 May, 2011, the soil sample was exposed to natural rainfall from 11h01 to 17h47. During the experiment, the soil sample was kept in its metal extraction casing and was tilted at 45° in order to obtain the same inclination as its in situ conditions.

The soil sample was scanned every 30 minutes using a ground-based TLS Leica ScanStation II, which produces point clouds (x, y, and z data) in a three-dimensional space (Figure 1c). The direction of the laser pulses' line-of-sight and the recorded time-of-flight determine the position of the measured points. The rainfall was measured by the weather station at the University of Lausanne (PluvioMADD2 from MADD Technology Sàrl, Yverdon-les-Bains, Switzerland), located 500 m from the experiment location.

The sample was dry at the beginning of the experiment. The total precipitation during the experiment was 5.5 mm, which corresponds to approximately 1.3 litres entering the metal case. Most of the rainfall was absorbed by the sediment, limiting the transport of sediment by runoff. Consequently, the sample did not reach full saturation. We suspect that a small quantity of evaporation may have occurred during the experiment, but we did not weigh the box before and after the experiment, and this minor influence has been neglected in our study.

3.3 Data acquisition

The surface evolution was monitored for 6 hours and 46 minutes by 12 successive laser scan acquisitions. The first scan and the last scan (acquired at 11h01 and 17h47, respectively) had a point spacing of approximately 0.001 m with a duration time of 8 min. All the other scans had a 0.002 m point spacing for a duration of 2 min. From 0 to 50 m, 50% of the laser beam is at a diameter of 4 mm at full width half height (FWHH) (Leica Geosystems AG, 2007). The scans were acquired vertically from left to right, which means that one centimetre in width is scanned in less than 2.4 s for the 2 min. scans and less than 9.6 s for the 8 min. scans. The scan distance was 2 m. The instrument was not moved throughout the experiment, meaning that the position and the orientation of the scans are identical for all acquisitions. Therefore, no scan alignment was necessary to compare the obtained point clouds.

3.4 Data processing

The point clouds were “manually” cleaned of the points that were not imaging the surface of the sample, i.e., the metal casing sides, the background of the scenery and several artefacts, including points not located on the terrain’s surface, such as rain drops. Only the surface of the sample was kept. Every cleaned scan has a very high point density: more than 400,000 points for the first and last acquisitions and a minimum of 110,000 points for the other scans (Table 1).

Each TLS point cloud was first rotated by 45° to obtain an approximately horizontal point cloud in order to interpolate in 2.5 dimensions. The interpolations were performed using an inverse distance method with a power of 1 (Shepard, 1968) via Surfer 8.0 software (GoldenSoftware, Golden, CO, USA). The point clouds were transformed into a regular squared grid of 1 mm for the first and last scans and 2 mm for the other datasets. This provided high-resolution digital elevation models (DEM) of altitude z above the mean horizontal surface. The search radius for DEM generation was defined as 1.5 times higher than the pixel size, i.e., 1.5 mm for scans with a point spacing of 1 mm and 3 mm for the scans with a point spacing of 2 mm (Figure 2). Although different values of DEM cell size were tested, this value was chosen as the most satisfactory compromise between accuracy and resolution. The generated DEMs were compared to quantify and map surface changes, i.e., mass movements and erosion/deposition processes. Each DEM was subtracted from the initial (or reference) DEM (DeRose et al., 1998). The resulting z difference grids have negative value pixels for "erosion" and positive value pixels for "deposition". To limit the noise of the measurements, absolute value differences less than 0.0015 m were ignored; this threshold was obtained by a trial and error procedure.

4 Results

The precipitation lasted from 13h30 until the end of the experiment, with a 30-minute hiatus starting at approximately 16h00. The maximum rainfall intensity (5.2 mm h^{-1}) occurred at 16h30. The cumulative precipitation quantity was 5.5 mm at the end of the experiment. Three different surface processes of topographic changes were identified. Figure 3 shows the difference between the initial and final scans (11h01 and 17h47, respectively). Changes in the surface elevation (z) appear in blue (increased elevation) and red (decreased elevation; Figure 3). We considered only the changes that are fully visible in the oblique view of the experiment (i.e., the box with a slope of 45°).

The micro-topographic changes that occurred along transect 1-2 are shown in Figures 3 and 4. Figure 4c shows a depression (in red) formed at the top of a small ridge, and the surface elevation of a depression below this ridge increased (in blue). This change can be interpreted as a downward mass movement at the millimetre scale. The small particles moved downward and filled a desiccation crack. This phenomenon occurred 30 minutes after the highest intensity rain event, between 17h00 and 17h30 (Figure 5).

When the rain intensity reached 1 mm h^{-1}, the entire surface of the soil started to rise (perpendicular to the surface of the 45° slope), which appears as a pale blue layer in Figures 3 and is illustrated in Figure 6. This process resulted in an overall rise of 1.5 to 3 mm over the course of the experiment, i.e., a cumulative 5.5 mm of rain (Figure 5). The surface elevation increased slowly after the first rain. At 16h30, the surface subsided, and the process was momentarily slowed down. Subsequently, the processes accelerated following the peak in rain intensity (Figure 5). Note that no significant rise in the topographic surface occurred at the top of the sample, which was protected from the rain (Figure 3).

Another observed process is linked to changes in the soil surface by lateral expansion (Figures 6 and 7). This process occurred continuously through the closing of desiccation cracks, which were present on the surface of the sample.

The final observed process was the stripping of soil particles by the kinetic energy of the raindrops. Although these changes were observed by the authors during the experiment, their magnitude was unfortunately too small to be significantly monitored by the TLS used in this study.

5 Discussion and conclusions

The topographic changes observed along transect 1-2 (Figures 3 and 4) occurred almost instantaneously, which excludes the rain splashing process. These changes are interpreted as a micro-landslide. Based on the duration of the scans and the size of the transported mass, we assume that it is highly unlikely that a scan had just crossed the region of interest when the movements occurred within it (0.05 m scanned in approximately 50 s). In addition, the two profiles before and after the occurrence of the changes mimic the profile changes usually observed in real landslides. The observed process is likely related to the initiation of miniature debris flows (MDFs) observed by Oostwoud Wijdenes and Ergenzinger (1998), but MDFs require heavy rainfall.

The observed rise in the surface, which occurred following a 30-minute delay after the initiation of rainfall, is certainly linked to the swelling of the material. The soil sample experienced swelling after the first rainfall intensity peak, contraction 30 minutes after the cessation of rainfall and renewed rising once the rain started again. This measured cyclic behaviour demonstrates that the swelling and contraction of the soil surface is a reversible process. We can assume that this process is linked to moderate rainfall intensities, which allow water to infiltrate the fine-grained material, causing swelling. This process is not necessarily caused by clay minerals because they are present only in small quantities (primarily illite) in the study area (Antoine et al., 1995). The swelling dissipates rapidly for moderate rainfall events because of the diffusion of water when the rainfall stops, which leads to a decrease in the effect of the water.

The crack-closing lateral expansion of the surface is also certainly linked to swelling but does not reverse when the rain stops. Figures 6 and 7 clearly show that the material has expanded and that the material as not transported because no deposition was observed at the bottom. We have not found any definitive explanation that accounts for the difference between the rising process and the lateral expansion process. However, the difference must be related to gravity, which increases the effect of swelling downward. When the two sides of the crack make contact, the moistened zone doubles its thickness, decreasing the water diffusion in the material. In addition, these processes must be components of creeping (Selby, 1993), likely because the retreat by drying is less effective in the downslope portion, leading to slow progressive downward movements.

The above interpretations are also important for the understanding of the infiltration process. Cracks clearly play an important role in the infiltration rates (Mitchell and van Genuchten, 1993; Römkens and Prasad, 2006) and consequently in the destabilisation of slopes (Stumpf et al., 2013; Galeandro et al., 2014). The processes analysed here play a role in the closure of cracks, as shown in Figure 7. In the present case study, we demonstrated how micro-scale infiltration can influence the degradation of soil surface by inducing downward mass movements that are not reversible.

We have also shown here the great potential of high-resolution three-dimensional TLS or photogrammetry point clouds for the analysis of the processes that lead to erosion through surface mass movements at the millimetre scale. Investigations of erosional processes using point clouds are increasing in number. These studies use laser scanners for either micro-scale surface imaging (Schmid et al., 2004; Barneveld et al., 2013) or measuring crack apertures (Sanchez et al., 2013). In addition, photogrammetry and structure from motion (SfM) methods are now being developed to analyse soil surfaces (Snapir et al., 2014).

This paper shows that monitoring the changes at the millimetre scale to examine soil surface changes and erosion is now possible. This development will aid in designing future experiments to analyse certain processes, such as swelling, crack closure, micro-landslides, and initiation of MDFs. With heavier rainfall, sediments will be mobilised and transported across longer distances, enabling the study of MDFs and the formation of rills. This study also demonstrates that material and rain intensity must be suitable to permit the efficient detection of rain splash processes and associated erosion; specifically, a rainfall intensity of greater than 20 mm h^{-1} is necessary (Mathys et al., 2005).

Acknowledgements

The authors would like to thank the *Observatoire de Recherche en Environnement* (ORE) of Draix for letting us sample soil in a protected area. We would also like to thank the UNIBAT service of the University of Lausanne (UNIL) for providing meteorological data from their weather station. We also greatly appreciate the comments and suggestions of our colleagues Drs. M.-H. Derron, Benjamin Rudaz and Antonio Abellán. We thank American Journal Experts for the improvements of the English language of this paper.

References

Antoine, P., Giraud, A., Meunier, M. and Van Asch, T.: Geological and geotechnical properties of the ‘terres noires’ in southeastern France: Weathering, erosion, solid transport and instability, Engineering Geology, 40, 223-234, 1995.

Barneveld, R.-J., Seeger, M. and Maalen-Johansen, I.: Assessment of terrestrial laser scanning technology for obtaining high-resolution DEMs of soils. Earth Surf. Process. Landforms, 38, 1096-9837, 2013.

Caris, J.P.T. and Van Asch, T.: Geophysical, geotechnical and hydrological investigations of a small landslide in the French Alps, Engineering Geology, 31, 249-276, 1991.

DeRose, R. C., Gomez B., Marden, M. and Trustrum, N. A.: Gully erosion in Mangatu Forest, New Zealand, estimated from digital elevation Models, Earth Surface Processes and Landforms, 23, 1045-1053, 1998.

Galeandro A., Doglioni A., Simeone V. and Šimůnek J. S.: Analysis of infiltration processes into fractured and swelling soils as triggering factors of landslides. Environ. Earth Sci. 71, 2911–2923, 2014.

Leica Geosystem AG: Leica ScanStation 2 technical note, Heerbrugg, Switzerland, Vl.07, 2007.

Malet, J.-P., Durand, Y., Remaître, A., Maquaire, O., Etchevers, P., Guyomarc’h, G., Déqué, M. and van Beek, L.P.H. Assessing the influence of climate change on the activity of landslides in the Ubaye Valley. In: McInnes, R., Jakeways, J., Fairbank, H., Mathie, E. (Eds): Proceedings of the International Conference on Landslides and Climate Change - Challenges and Solutions, Taylor & Francis, London, pp. 195-205, 2007.

Maquaire O., Ritzenthaler A., Fabre D., Ambroise B., Thiery Y., Truchet E., Truchet E., Malet J.-P. Caractérisation des profils de formations superficielles par pénétrometrie dynamique à énergie variable: application aux marnes noires de Draix (Alpes-de-Haute-Provence, France). Comptes Rendus Géosciences, 334, 835–841, 2002.

Mathys N., Klotz S., Esteves M., Descroix L. and Lapetite J.-M.: Runoff and erosion in the Black Marls of the French Alps: observations and measurements at the plot scale. Catena, 63, 261-281, 2005.

Mitchell AR AND van Genuchten MTh. Flood irrigation of a cracked soil. Soil Science Society of America Journal. 57, 490–497, 1993.

Oostwoud Wijdenes, D.J. and Ergenzinger, P.: Erosion and sediment transport on steep marly hillslopes, Draix, Haute-Provence, France: an early experimental field study. Catena, 33, 179-200, 1998.

Römkens M.J. M. and Prasad, Rain Infiltration into swelling/shrinking/cracking soils. Agricultual Water Management 86, 96 – 205, 2006.

Sanchez M., Atique A., Kim S., Romero E. and Zielinski M. Exploring desiccation cracks in soils using a 2D profile laser device. Acta Geotechnica, 8, 583–596, 2013.

Schmid, T., Schack-Kirchner, H. and Hildebrand, E.: A Case Study of Terrestrial Laser-Scanning in Erosion Research: Calculation of Roughness Indices and Volume Balance at a Logged Forest Site. Eds: M. Thies, B. Koch, H. Spiecker and H. Weinacker: Laser-Scanners for Forest and Landscape Assessment. ISPRS Archives – V. XXXVI-8/W2 - WG VIII/2, 114-118, 2004.

Selby, M.J., Hillslope materials and processes: Oxford, UK, Oxford University Press, 252–258, 1993.

Shepard, D., A two dimensional interpolation function for irregularly-spaced data, New York, USA. Proceeding ACM '68 Proceedings of the 1968 23rd ACM national conference, 517-524 1968.

Snapir B., Hobbs S. and Waine T.W. Roughness measurements over an agricultural soil surface with Structure from Motion. ISPRS J. of Photogrammetry and Remote Sensing, 96, 210–223, 2014.

Stumpf, A., Malet, J.-P., Kerle, N., Niethammer, U., & Rothmund, S. Image-based mapping of surface fissures for the investigation of landslide dynamics. Geomorphology, 186, 12-27, 2013.

Torri, D., Regüés, D., Pellegrini, S. and Bazzoffi P.: Within-storm surface dynamics and erosive effects of rainstorms. Catena, 38, 131-150, 1999.

Table 1: Summary of the TLS scans in the TLS campaign experiment on 31 June, 2010. This table compiles the information concerning the scan time, the number of points before and after cleaning, the mean spacing between the points and the density of points.

Start of acquisition (duration [min])	Number of points before cleaning	Mean spacing [mm]	Distance from TLS [m]	Number of points after cleaning	Density [pts/cm^2]
11h01 (8)	601349	1	2	496391	84.84
12h00 (2)	149951	2	2	123233	21.06
14h00 (2)	149951	2	2	123477	21.10
14h30 (2)	149951	2	2	123269	21.07
15h00 (2)	149951	2	2	123496	21.11
15h30 (2)	149951	2	2	122857	21.00
16h00 (2)	149951	2	2	120162	20.54
16h30 (2)	149951	2	2	118301	20.22
17h00 (2)	149951	2	2	117290	20.05
17h30 (2)	149951	2	2	116322	19.88
17h32 (8)	601349	1	2	467484	79.90
17h47 (8)	601349	1	2	469906	80.31

Figure 1: a. View of the sample collection process, the metal case (1 m x 0.5 m x 0.20 m), and the approximate orientation of the bedding. The bottom plate is partially inserted. b: View of the soil sample with an inclination of 45° during the rainfall event. c. Position of the TLS, which is protected from rainfall by a tent, relative to the metal case.

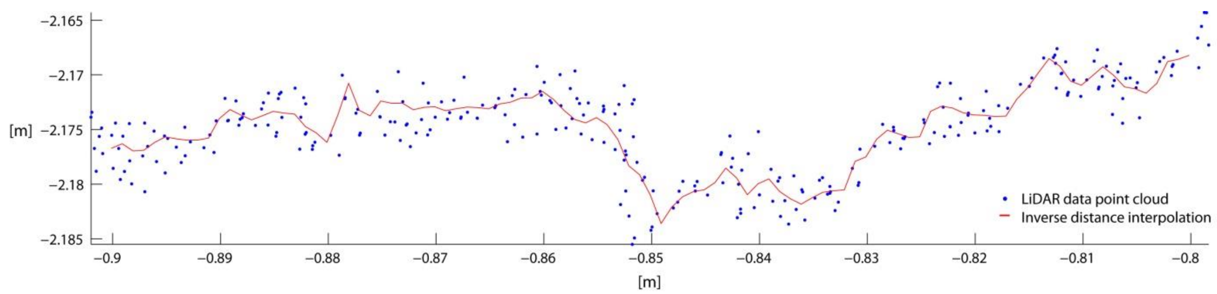

Figure 2: A 10-cm-long downhill section using the points from a 1-cm-wide swath of the original TLS data point cloud compared with the 1 mm DEM profile (17h47 scan data). The profile has been processed with an inverse distance interpolation with a power of one.

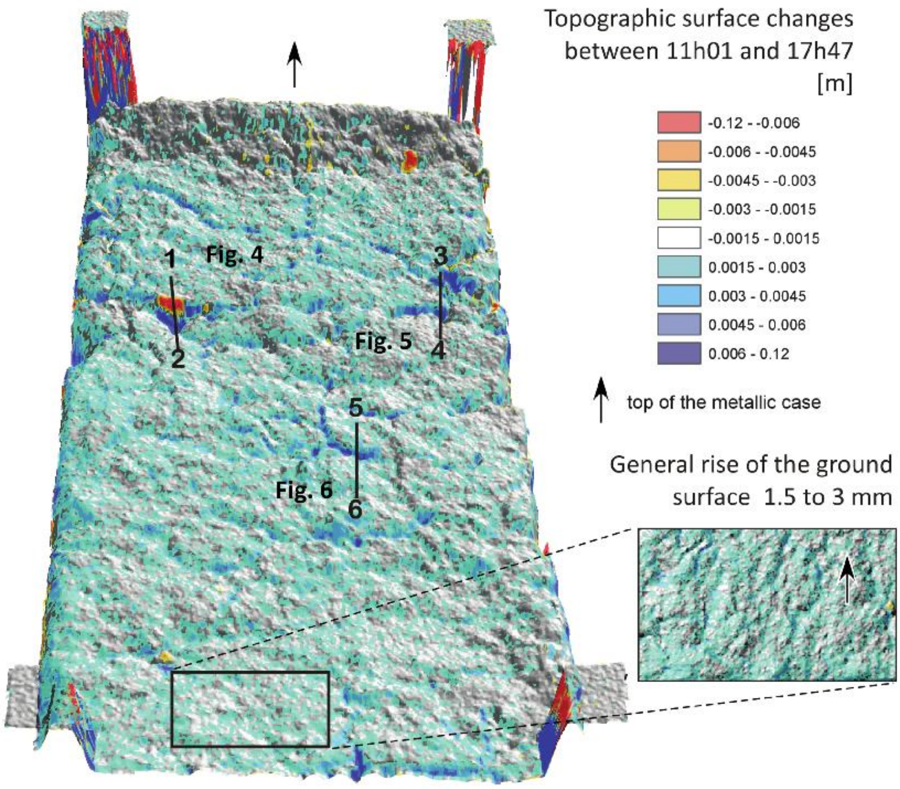

Figure 3: A comparison of TLS scans. The colours represent topographic changes between 11h01 and 17h47. The figure also includes a detailed view of the surface. The locations of Figures 4 to 6 are indicated.

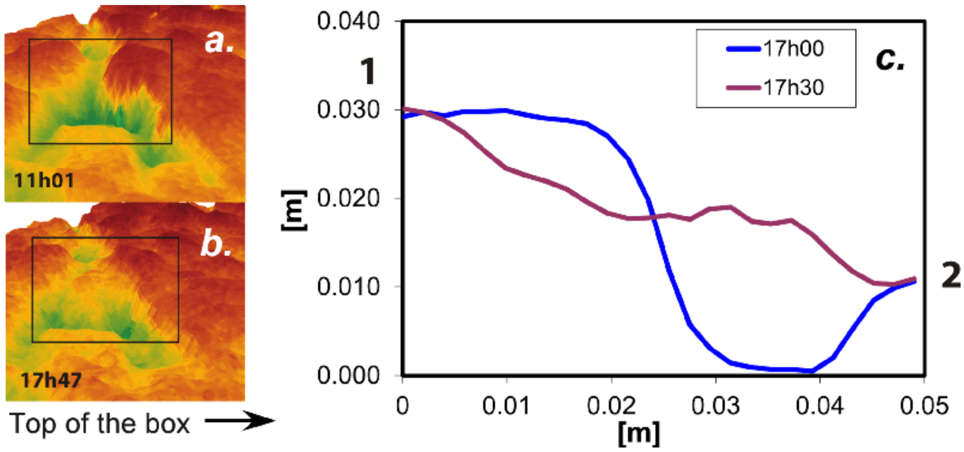

Figure 4: Profile changes showing mass movement occurring between 17h00 and 17h30. a. A 3D view of the zone at 11h01 and b. at 17h47. The black boxes indicate the position of the profiles in c.

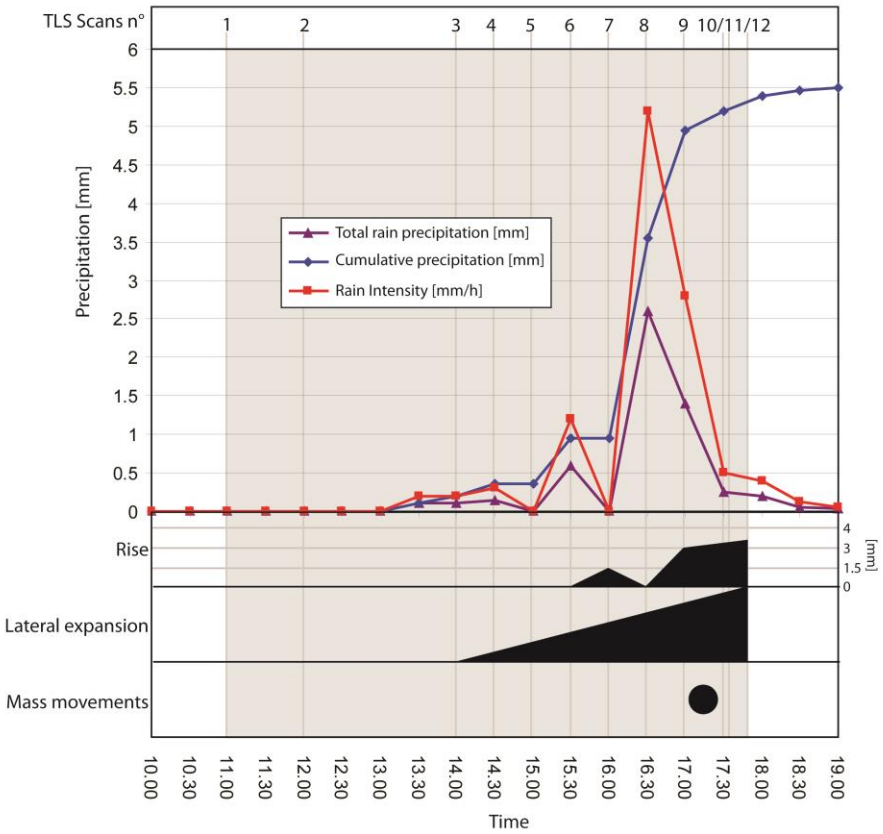

Figure 5: Observed phenomenon relative to the precipitation data. The total rain amount in mm, the cumulative precipitation and the rain intensity are presented. The rise is shown in mm, and the lateral expansion intensity and mass movement processes are presented in relative scales.

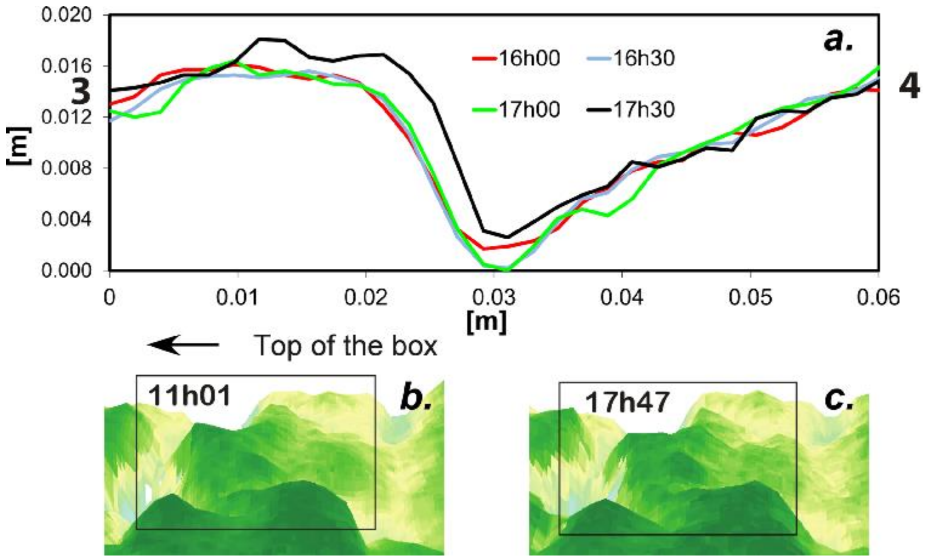

Figure 6: a. Profile changes showing the evolution of lateral expansion and surface rise between 16h00 and 17h30. b. A 3D view of the zone at 11h01 and b. at 17h47. The black boxes indicate the position of the profiles in a.

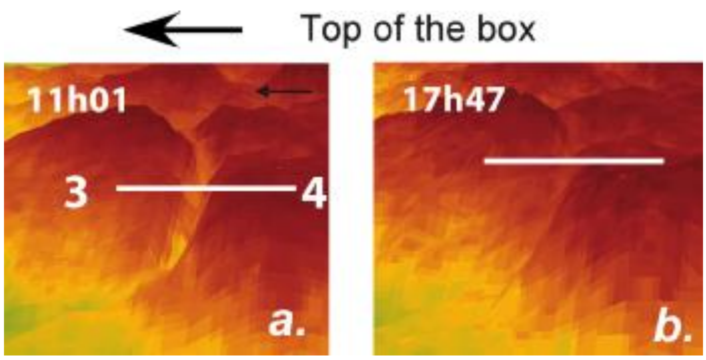

Figure 7: 3D views of the evolution of lateral expansion, which closes a crack between 11h01 (a) and 17h47 (b).